SVN Stroke & Vascular Neurology

Low-intensity focused ultrasound stimulation promotes stroke recovery via astrocytic HMGB1 and CAMK2N1 in mice

Lin Qi,[1] Cheng Wang,[1] Lidong Deng,[1] Jia-Ji Pan,[2] Qian Suo,[1] Shengju Wu,[1] Lin Cai,[3] Xudong Shi,[4] Junfeng Sun,[1] Yongting Wang ,[1] Yaohui Tang,[1] Weibao Qiu,[4] Guo-Yuan Yang ,[5,6] Jixian Wang ,[6] Zhijun Zhang[1]

To cite: Qi L, Wang C, Deng L, *et al*. Low-intensity focused ultrasound stimulation promotes stroke recovery via astrocytic HMGB1 and CAMK2N1 in mice. *Stroke & Vascular Neurology* 2024;**9**: e002614. doi:10.1136/svn-2023-002614

► Additional supplemental material is published online only. To view, please visit the journal online (http://dx.doi.org/10.1136/svn-2023-002614).

Received 25 May 2023
Accepted 28 November 2023
Published Online First 8 January 2024

For numbered affiliations see end of article.

Correspondence to
Professor Zhijun Zhang; zhangzj@sjtu.edu.cn

Dr Jixian Wang; wangjixian6@163.com

ABSTRACT

Background Low-intensity focused ultrasound stimulation (LIFUS) has been developed to enhance neurological repair and remodelling during the late acute stage of ischaemic stroke in rodents. However, the cellular and molecular mechanisms of neurological repair and remodelling after LIFUS in ischaemic stroke are unclear.

Methods Ultrasound stimulation was treated in adult male mice 7 days after transient middle cerebral artery occlusion. Angiogenesis was measured by laser speckle imaging and histological analyses. Electromyography and fibre photometry records were used for synaptogenesis. Brain atrophy volume and neurobehaviour were assessed 0–14 days after ischaemia. iTRAQ proteomic analysis was performed to explore the differentially expressed protein. scRNA-seq was used for subcluster analysis of astrocytes. Fluorescence in situ hybridisation and Western blot detected the expression of HMGB1 and CAMK2N1.

Results Optimal ultrasound stimulation increased cerebral blood flow, and improved neurobehavioural outcomes in ischaemic mice ($p<0.05$). iTRAQ proteomic analysis revealed that the expression of HMGB1 increased and CAMK2N1 decreased in the ipsilateral hemisphere of the brain at 14 days after focal cerebral ischaemia with ultrasound treatment ($p<0.05$). scRNA-seq revealed that this expression pattern belonged to a subcluster of astrocytes after LIFUS in the ischaemic brain. LIFUS upregulated HMGB1 expression, accompanied by VEGFA elevation compared with the control group ($p<0.05$). Inhibition of HMGB1 expression in astrocytes decreased microvessels counts and cerebral blood flow ($p<0.05$). LIFUS reduced CAMK2N1 expression level, accompanied by increased extracellular calcium ions and glutamatergic synapses ($p<0.05$). CAMK2N1 overexpression in astrocytes decreased dendritic spines, and aggravated neurobehavioural outcomes ($p<0.05$).

Conclusion Our results demonstrated that LIFUS promoted angiogenesis and synaptogenesis after focal cerebral ischaemia by upregulating HMGB1 and downregulating CAMK2N1 in a subcluster of astrocytes, suggesting that LIFUS activated specific astrocyte subcluster could be a key target for ischaemic brain therapy.

WHAT IS ALREADY KNOWN ON THIS TOPIC

⇒ Low-intensity focused ultrasound stimulation (LIFUS) has been developed to enhance neurological repair and remodelling of ischaemic stroke in rodents.

WHAT THIS STUDY ADDS

⇒ This study showed that 3 min with 101 mW/cm^2 every other day of ultrasound stimulation increased angiogenesis and synaptogenesis at the late acute stage of stroke recovery. Increased HMGB1 and decreased CAMK2N1 derived from astrocytes may be key ultrasound therapeutic targets.

HOW THIS STUDY MIGHT AFFECT RESEARCH, PRACTICE OR POLICY

⇒ This study will provide innovative therapeutic targets by ultrasound for ischaemic stroke recovery at the late acute stage.

INTRODUCTION

Stroke is the second leading cause of death and the leading cause of disability globally.[1] After a stroke, the neurovascular unit was disrupted, leading to an injury to capillaries and neurons, and loss of synapses, causing brain injury and impairing long-term motor and cognitive function. Even if patients are treated in the acute phase, they also faced long-term injuries.[2–4] Therefore, in addition to the treatment in the acute stage, delayed therapies aimed to repair neurovascular units are also potentially significant and urgent needs after stroke.

Recently, neuromodulation techniques mainly including transcranial magnetic stimulation, transcranial electrical stimulation and transcranial focused ultrasound[5] have been developed. Among them, TUS showed the great advantage of high spatial specificity, high penetration depth and non-invasive properties, which widely attracted the attention of neurobiologists.[6–9] Ultrasonic stimulation of the frontal–temporal cortex significantly improved the patient's mental status and pain, and further reduced ischaemic injury.[10 11] Ultrasonic neuromodulation

significantly decrease parkinsonian-related activity in mice models[12] and focused ultrasound thalamotomy treatment was approved by FDA for patients with essential tremor who did not respond to medication.[13] These results suggested that cell-type-specific activation combined with Ca^{2+}-dependent molecular pathways could be expanded to pathological conditions. Motor function, neural activity and haemodynamic responses showed a linear coupling with ultrasound stimulation of the mouse cortex.[9] Incomplete motor function recovery was one of the major pathological features of ischaemic stroke, and low-intensity focused ultrasound stimulation (LIFUS) has been shown to promote neurorehabilitation after ischaemic stroke.

The promotion of angiogenesis and neurogenesis is the main targets for the later stage of stroke therapy. Synaptogenesis is a cardinal component of neurogenesis. LIFUS was shown to modulate brain activity, with the most focused on the induction of motor responses and neuromodulation function.[9] Recently, the promotion of angiogenesis and neurogenesis by LIFUS was demonstrated in many experiments in vitro and in vivo with a variety of parameters.[14–17] In vitro, LIFUS was proved to promote the secretion of neurotrophic factors from astrocytes such as vascular endothelial growth factor (VEGF) and brain-derived growth factor (BDNF).[18 19] In vivo, LIFUS could induce angiogenesis to ameliorate infarction area in the acute stage of stroke, and inhibit brain oedema formation.[20–22] These studies intrigued us to explore which optimal parameter of LIFUS would be suitable for late-stage therapy for ischaemic stroke and its underlying mechanism.

Here, we investigated the effects and molecular mechanisms of LIFUS in angiosynaptic regeneration after 7 days of ischaemic stroke in mice.

MATERIALS AND METHODS

Parameters of LIFUS including stimulation frequency, intensity, duration and relative protocols were generated and listed as shown in the online supplemental materials. For in vivo experiments, mice (n=120) were randomly allocated into experimental treatment or control groups, and n=12 mice per group were analysed for neurobehavioural tests and laser speckle imaging; other experiments were around n=4 mice per group, the details we put in the online supplemental materials. Animal experiments were planned using G*Power software (Heinrich-Heine-Universität Düsseldorf, V.3.1.9.6, setting α at 0.05 and power at 0.8) combined with the pre-experiment to determine sample size. Adult male mice (8–10 weeks, C57BL/6J) were used for MCAO and other experiments, and aged male mice were 22 months. Animals were randomly distributed into required groups receiving either scramble or the pAAV viral inhibitor or overexpression, in each intervention test, and a control group was performed to fulfil reconfirmation. Endpoints for the animal experiments were determined in accordance with institutionally approved criteria.

For the specific analysis of the underlying molecular mechanisms in MCAO mice following LIFUS, multiomics approaches including iTRAQ proteomic analysis were performed to detect the key different proteins and pathways, and single-cell RNA sequencing analysis was performed to identify the potential clusters of different cell types and groups. For functional outcomes, laser speckle imaging, electromyography (EMG) and fibre photometry records were applied at different time points in MCAO mice.

Last, proof-of-concept studies were performed in vivo. Outcomes were determined by assessing molecular factors, histological phenotype, electrophysiology and neurobehavioural function performed in a blinded manner 14 days after the ischaemic brain injury. The molecular mechanisms in the ipsilateral hemisphere in response to LIFUS were determined by Fluorescence in situ hybridisation (FISH), immunofluorescence staining, qPCR, Western blot and corresponding quantification. All analyses were performed in an unbiased fashion. The details of methods are mainly presented in the online supplemental materials.

RESULTS

Optimised LIFUS parameters for ischaemic stroke therapy in mice

Experiments were designed as shown in online supplemental figure 1. A LIFUS with 500 kHz centre frequency was suitable for rodent research (Ultrasound Neurostimulation System, Shenzhen Institute of Advanced Technology, Chinese Academy of Sciences, Shenzhen, China). The x-y diameter of ultrasound was 4.5 mm and 5 mm, respectively, the depth of ultrasound irradiation was 4 mm, and the x-y diameter was 2 mm when normalised sound pressure was more than 50% of total irradiation energy (figure 1A–C). The sequence diagram of the ultrasound stimulation was shown. 500 kHz pulse repetition frequency (PRF), 300 ms sonication duration (SD) and 50% duty cycle (DC)[23] were used across all the ultrasound experiments (figure 1D).

Additional combinations of pressure (MPa) were used to make I_{spta} different (online supplemental table S1). We combined different ultrasonic intensity (UI: 22, 101, 201 mW/cm^2) and stimulation duration (1, 3, 5 min) to treat stroke mice in the late acute stage (online supplemental table S2). We measured the cerebral blood flow (CBF) after ultrasound stimulation using laser speckle imaging. The result showed that CBF increased after immediate ultrasound stimulated ipsilateral hemisphere for 3 or 5 min with 101 and 201 mW/cm^2 day 7 after stroke (online supplemental figure 2A). The motor function was evaluated by modified neurological severity score (mNSS) before and up to 14 days after MCAO using different stimulation parameters, results showed that only 101 mW/cm^2 improved neurobehavioural outcomes. One day of

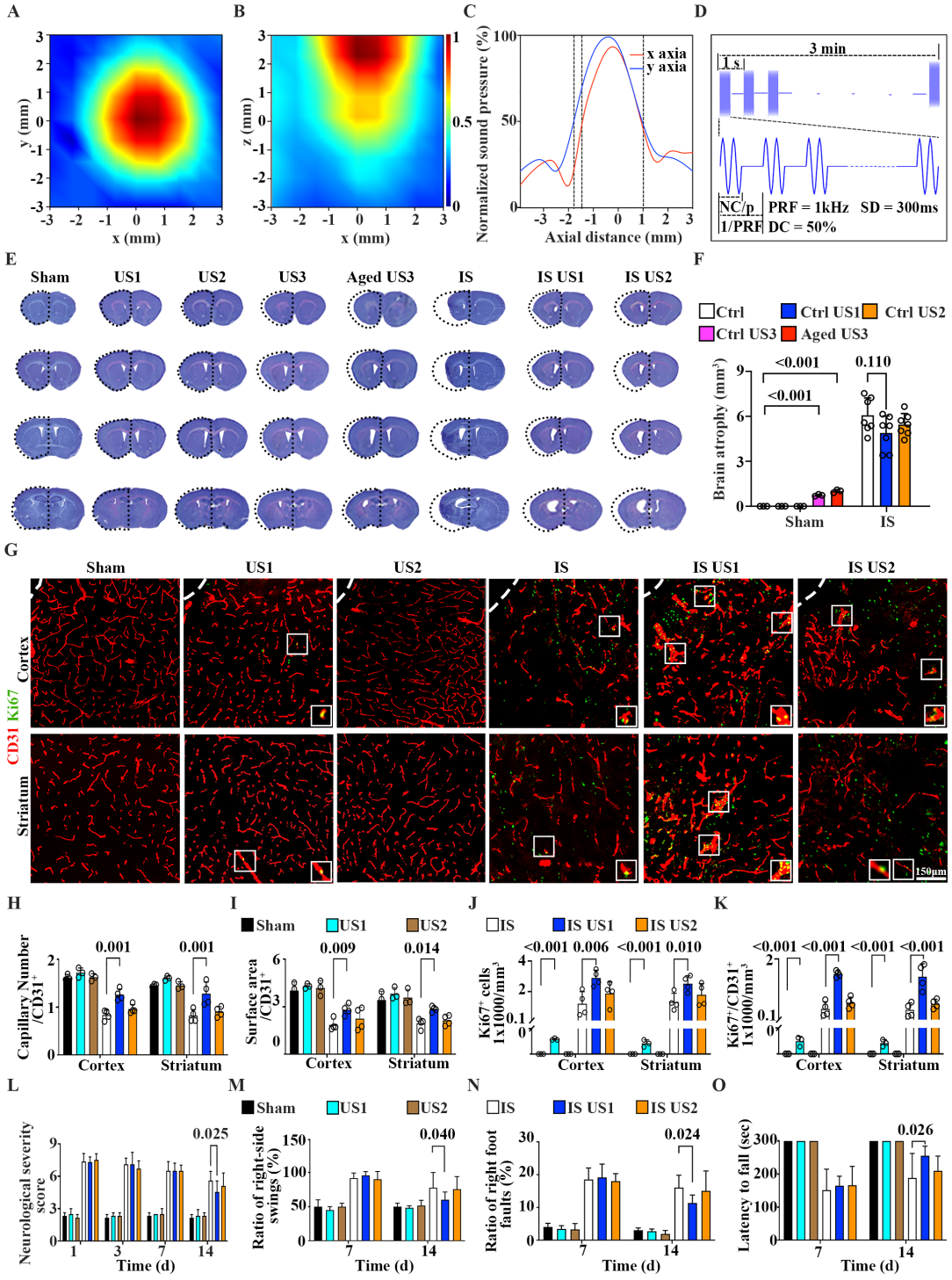

Figure 1 Establishing optimal LIFUS parameters for neuronal repair and remodelling in MCAO mice. (A) 2D distribution of the ultrasound field in oblique and longitudinal cross-sections. The x-axis and y-axis of the ultrasound spot were ~4.5 mm and ~5 mm, respectively. (B) Depth of ultrasound irradiation was 4 mm. (C) X-Y diameter was 2 mm when normalised sound pressure was more than 50% of the total irradiation energy. (D) Schematic diagram of ultrasound, PRF was 1 kHz and 1/PRF was 1 s, SD was 300 ms, and DC was 50%. (E) Cresyl violet-stained brain sections and (F) quantification of atrophy volume at 14 days following MCAO. Dashed lines indicated brain atrophy area, (n=3–7 mice/group). (G) Representative CD31 (red) and Ki67 (green) immunostaining images in the perifocal region. (H) Quantitative analysis of capillary number, (I) surface area, (J) Ki67$^+$, and (K) Ki67$^+$/CD31$^+$ signals in the perifocal region of ipsilateral hemisphere after 14 days following MCAO in mice, (n=4 mice/group. Scale bar=150 μm). (L) mNSS, (M) tail suspension, (N) grid walking and (O) rotarod test for neurobehavioural outcomes in each group (n=3 mice/group in sham groups, n=10–12 mice/group in the IS groups). US1, –2 to –3=mice treated with different dose of ultrasound. IS, ischaemic stroke mice; IS US, ischaemic stroke mice treated with US. Data are mean ± SD. LIFUS, low-intensity focused ultrasound stimulation; mNSS, modified neurological severity score; PRF, pulse repetition frequency; SD, sonication duration.

ultrasound stimulation interval and 3 or 5 min of stimulation duration achieved a better recovery in neurobehavioural outcomes compared with the MCAO mice (IS, online supplemental figure 2B–D).

To explore whether longer time of ultrasound stimulation would have better or side effect in MCAO mice, we added a group of 10-min stimulation with 101 mW/cm^2 every other day. Then, we labelled ultrasound stimulation 3, 5 and 10 min with 101 mW/cm^2 every other day as US1, US2 and US3, respectively (online supplemental table S3). We examined the brain atrophy volume to further determine the appropriate ultrasound parameter (figure 1E). Cresyl violet staining results showed that US3 damaged the ipsilateral hemisphere in both young and aged healthy mice compared with the control, indicated that 10 min was an overtime of stimulation. For MCAO (IS) groups, US1 showed better potential than US2 to reduce the brain atrophy volume (figure 1F). The instant change of CBF and mNSS results showed that US1 and US2 were better stimulation to improve stroke recovery. To explore the effect of LIFUS on CBF of MCAO mice, we measured the spatiotemporal changes of CBF using laser speckle imaging, and chose the perifocal regions as ROI (online supplemental figure 2E). For the sham group, there was no difference in CBF changes in immediate, 7 and 13 days, and 13 days endpoint after US1 and US2. For the IS groups, both US1 and US2 groups of mice showed better CBF recovery in the ipsilateral hemisphere of the IS mice than that of IS group, while US1 exhibited increased CBF at day 7 to the endpoint of 13 days after MCAO (online supplemental figure 2F).

The increase of cerebral blood volume is attributed to a surge of angiogenesis.[24 25] We investigated angiogenesis in the perifocal region of the ipsilateral hemisphere after MCAO (figure 1G). The number of microvessels and surface CBF did not increase in the sham groups after US1 or US2 treatment (figure 1H,I). The number of Ki67$^+$ cells and Ki67$^+$/CD31$^+$ microvessels increased in perifocal region of the ipsilateral hemisphere at 14 days of MCAO after US1 or US2 treatment, but they were more prominent after US1 treatment (figure 1J,K).

To further determine which was the best stimulation parameter of LIFUS for the neurobehavioural recovery in the MCAO mice, we applied a number of neurobehavioural tests including mNSS, tail suspension test, foot fault and rotarod to comprehensively evaluate the sensorimotor functions up to 14 days after MCAO (figure 1L–O). Both US1 and US2 stimulation did not induce significant change compared with that in the sham groups. For IS groups, both US1 and US2 showed better outcomes than that in IS groups, while US1 exhibited fewer motor deficits and better neurological recovery in all the four neurobehavioural tests in the MCAO mice (figure 1L–O). qPCR results also showed that mRNA level of VEGF, BDNF and endothelial nitric oxide synthase (eNOS) increased in the MCAO mice after US1 stimulation compared with the IS group (online supplemental figure 2G). Taken together, these data suggested that US1 stimulation attenuated neurological deficits and promoted functional recovery at both the histological and neurobehavioural levels. Therefore, US1 was chosen as the optimal ultrasound stimulation method in the following experiments.

LIFUS upregulated HMGB1 and downregulated CAMK2N1 in a new cluster of astrocytes

To explore the mechanism of ultrasound effect on CBF recovery and newly formed microvessels, we performed iTRAQ-based proteomic analysis to detect the mechanism in the protein level. Genes with a p value<0.05 and |fold change|≥1.5 were regarded as DEGs. Overall, 261 genes were upregulated and 848 genes were downregulated after LIFUS compared with the IS mice (online supplemental figure 3A). Volcano plot displayed 184 genes involved in angiogenesis and synapse pathway (figure 2A). We further conducted gene ontology (GO) pathway analyses to display the enrichment of 15 terms clustering from all different expression genes that we were interested in the IS US group compared with the IS group, indicating that ultrasound truly change the physiological process after ischaemic stroke significantly, and correlated to VEGF and calcium related pathways (figure 2B). Heatmap displayed changed genes, which related with angiogenesis and synapse signal pathways in the IS US group compared with the IS group (figure 2C).

To further explore the mechanism at single-cell level, cell lineage analysis by comprehensive single-cell RNA-sequencing was performed to gain information of the transcriptional profile in different treated groups. Cluster analysis using a uniform manifold approximation and projection for dimension reduction (UMAP) revealed the difference in global gene expression profiles of cell types in four different groups, and identified clusters of cells with unique genetic signature (figure 2D, online supplemental figure 3B). Gene expression profiles of healthy and injured region with or without ultrasound stimulation were shown by UMAP, suggesting that the expression profiles after LIFUS both in physiological and pathological conditions were different (online supplemental figure 3C).

Since previous studies showed that astrocyte mediated the effects of ultrasonic neuromodulation, we then concentrated on the subclusters of astrocytes in four groups of astrocytes. Heatmap showed 17 differentially expressed genes overlapped with genes of iTRAQ proteomic analysis related to angiogenesis and synapse pathways in astrocytes of the IS US mice compared with that in the IS mice (figure 2E). We found that most of the other significantly differential genes were phenotypic genes such as Pecam1 or pathway genes such as Pik3c2a/Atp5f1d. We aimed to find the initial genes that directly response to ultrasound as the target genes therefore, then focused on HMGB1 and CAMK2N1. HMGB1 was the top differential expressed gene related to angiogenesis, and CAMK2N1 was the top differential gene related to synaptogenesis, suggesting that these two genes were

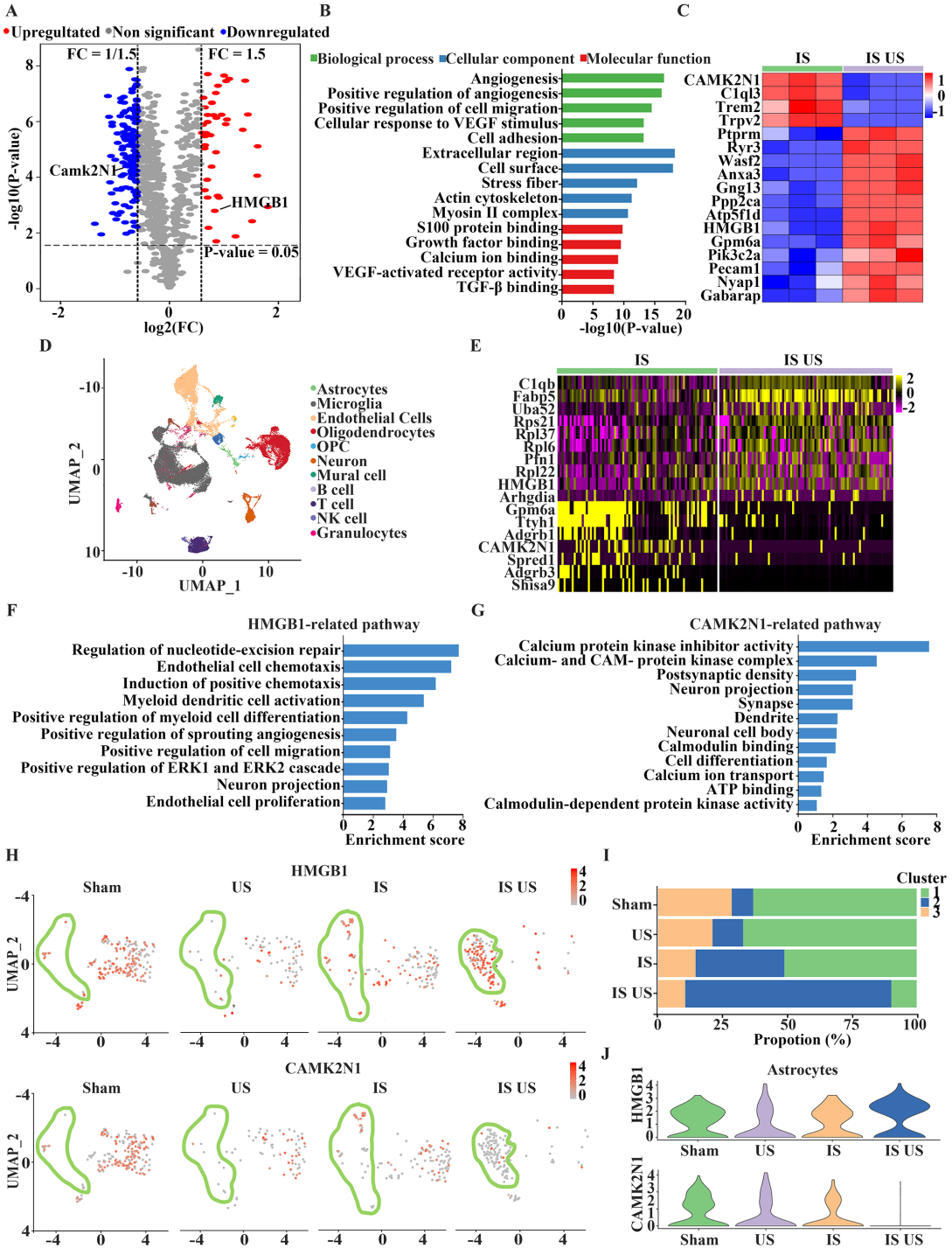

Figure 2 LIFUS upregulated HMGB1 and downregulated CAMK2N1 in a new cluster of astrocytes. (A) Volcano plot demonstrated fold change of protein level of HMGB1and CAMK2N1 in the IS US group compared with the IS group. (B) Bar chart of GO terms showed angiogenesis and synapse related pathways including BP (biological process, green), CC (cell component, blue), and MF (molecular function, red). (C) Heatmap showed different protein expression in the IS US group compared with IS group. (D) UMAP plot showed the expression profiles in the left ipsilateral by clustering cell types in the ipsilateral hemisphere of mouse brain. (E) Heatmap showed differentially expressed genes (DEGs) in the IS US group compared with IS group of astrocytes. (F) Bar chart of GO terms showed enriched HMGB1 and (G) CAMK2N1-related pathways of astrocytes in the IS US group. (H) Expression profiles of HMGB1 and CAMK2N1 in astrocytes organised into groups, and coloured based on gene expression patterns. (I) Bar chart showed the proportions of three subgroups in four different groups. (J) Violin plots represented the expression distributions of HMGB1 and CAMK2N1 in astrocytes organised into groups. GO, gene ontology; IS, ischaemic stroke mice; IS US, ischaemic stroke mice treated with US; US, mice treated with ultrasound; LIFUS, low-intensity focused ultrasound stimulation; UMAP, uniform manifold approximation and projection; VEGF, vascular endothelial growth factor.

involved in the promotion of angiogenesis and synaptogenesis in MCAO mice with LIFUS. Bar chart of GO terms showed enriched HMGB1 and CAMK2N1-related pathways in astrocytes from IS US group, including angiogenesis-related, calcium-related and synapse-related pathways which we focused on (figure 2F,G). The secondary profiling of astrocytic subclusters yielded three subtypes with distinct functional cell identities (online supplemental figure 3D). Feature plot showed HMGB1 and CAMK2N1 expression in secondary profiles of four different groups (figure 2H). Among the three subclusters, the proportion of subcluster 2 (C2) astrocytes in the IS US mice was~70%, more than IS group (figure 2I), suggesting that IS US promote the C2 positive new subcluster. Heatmap showed expressed genes that HMGB1 increased and CAMK2N1 decreased in subcluster 2 compared with other subclusters (1 and 3) in astrocytes, which was consistent with iTRAQ proteomics analysis (online supplemental figure 3E). The distributions of HMGB1 and CAMK2N1 expression in astrocytes, microglia and endothelial cells were displayed by violin plots (figure 2J, online supplemental figure 3F). Heatmap of top differentially expressed genes in astrocytes related to angiogenesis and synapse pathway were shown in the US group compared with sham group, while there has no change of HMGB1 and CAMK2N1 expression (online supplemental figure 3G). GO terms displayed enriched pathways in all cell types in US group compared with the sham group, and showed that enriched C2 promote angiogenesis, neuroregeneration, immune and inflammatory related pathways after stroke, and other cell types could be involved in angiogenesis and synaptogenesis via different signal molecules in physiological condition (online supplemental figure 3H).

Astrocytic HMGB1 inhibition decreased angiogenesis-related factor expression and reversed neurobehaviour recovery after LIFUS in MCAO mice

To investigate whether LIFUS increased angiogenesis by upregulating HMGB1 in astrocytes of MCAO mice, we knocked down HMGB1 in whole-brain cells by pAAV-U6-shRNA (HMGB1)-CMV-WPRE virus, and in astrocytes by pAAV-GfaABC1D-3xFLAG-miR30shRNA (HMGB1)-WPRE virus. pAAV-U6-shRNA-CMV-WPRE virus was used as a control.

FISH was used to colocalise targeted gene with astrocytes in RNA level. FISH results showed that HMGB1 significantly expressed in astrocytes compared with the corresponding controls at 14 days after MCAO (figure 3A). Expression of HMGB1 increased after US treatment compared with the IS group of mice and decreased in the IS US sh (HMGB1 inhibition in the whole brain) and IS US gf-sh groups (HMGB1 inhibition in astrocytes) in mRNA level (figure 3B), which demonstrated that viral inhibition was effective. By quantifying the number of $HMGB1^+/GFAP^+$ astrocytes in the perifocal region at 14 days after MCAO by FISH, we found that 64% of $HMGB1^+$ cells were astrocytes and 36% $HMGB1^+$ cells were other type of cells (figure 3C).

We then analysed the expression of HMGB1, VEGFA and FGF2 in perifocal regions in MCAO mice. VEGFA and FGF2 expression showed an increasing trend in the sham group after LIFUS. The expression of HMGB1, VEGFA and FGF2 significantly increased in LIFUS treated groups compared with the IS group at 14 days after MCAO, which was reversed by HMGB1 inhibition in IS US sh and IS US gf-sh groups of mice (figure 3D,E). The expression of other proteins and neurobehavioural outcomes was not affected by HMGB1 inhibition in the sham mice (online supplemental figure 4A-F). For IS groups, ultrasound-treated groups showed better neurobehavioural outcomes including mNSS, tail suspension test, foot fault and rotarod than that in the IS group at 14 days after MCAO (figure 3F–I), and reversed by the inhibition of HMGB1 in the whole brain and astrocytes.

LIFUS-upregulated HMGB1 in astrocytes promoted CBF and $lectin^+$ microvessels after MCAO

To determine whether LIFUS-induced angiogenesis was correlated with upregulated HMGB1 in astrocytes, we further measured the spatiotemporal changes of CBF and brain microvasculature in ipsilateral perifocal region (figure 4). Surface CBF increased in the IS US group compared with the IS group of mice (figure 4A,B). We also qualified the ratio of the ipsilateral to the contralateral of ROI; the results also showed that CBF increased at day 7 and day 13 after MCAO (figure 4). Increased CBF induced by LIFUS were reversed by inhibiting HMGB1 in the whole brain cells as well as astrocytes (figure 4A,B).

We further investigated functional angiogenesis by injecting tomato lectin. $Lectin^+$ microvessels increased in the IS US group compared with IS group of mice which was reversed after HMGB1 inhibition (figure 4C). The quantification of $lectin^+$ capillary number and surface area increased in the US groups compared with the IS, IS US sh and IS US gf-sh groups (figure 4D,E). $Ki67^+$ cells colabelled with $lectin^+$ microvessels emerged in the perifocal regions, indicating newly formed microvessels. $Ki67^+$ cells and $Ki67^+/lectin^+$ microvessels increased in the perifocal region of the IS US group of mice compared with the other 3 groups of mice at day 14 following MCAO (figure 4F,G). scRNA results showed that HMGB1 mRNA has no difference in sham groups with or without US treatment (online supplemental figure 3G), suggesting that ischaemic mice easily respond to LIFUS, and finally led to improve outcomes.

Astrocytic CAMK2N1 overexpression reversed the synapses increase after LIFUS in MCAO mice

To determine whether LIFUS promoted synaptogenesis via decreasing CAMK2N1 in astrocytes after MCAO, we overexpressed CAMK2N1 in the brain cells by pAAV-CAG-P2A-CAMK2N1-3xFLAG-WPRE and in astrocyte by pAAV-GfaABC1D-P2A-CAMK2N1-3xFLAG-WPRE. pAAV-P2A-3xFLAG-WPRE was used as a control.

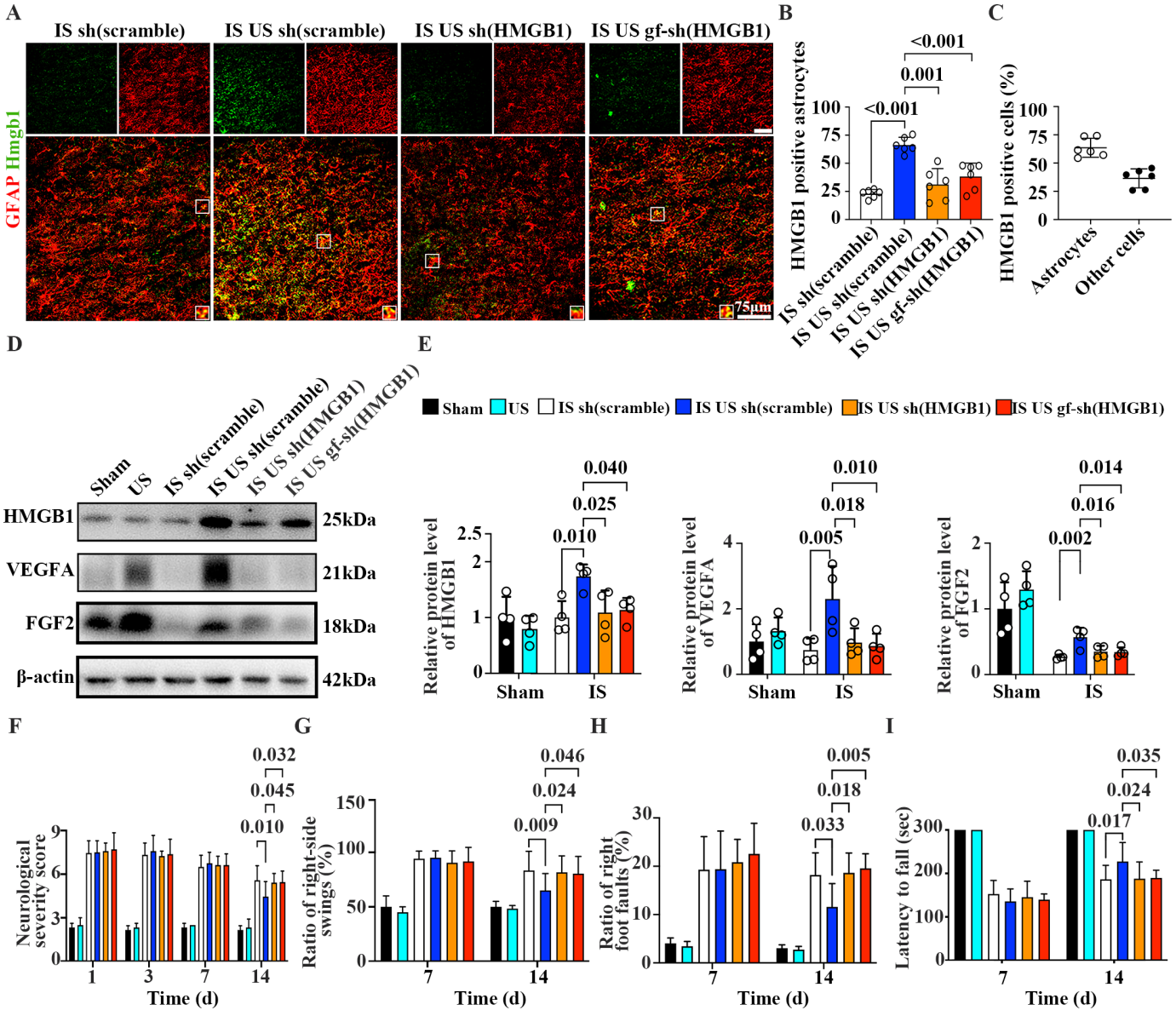

Figure 3 Inhibiting astrocytic HMGB1 attenuated angiogenesis and reversed neurobehavioural outcomes after LIFUS in MCAO mice. (A) Representative in situ hybridisation images of HMGB1 (green) signals and GFAP$^+$ astrocytes (red) in the IS scramble, IS US scramble, IS US sh (HMGB1), and IS US gf-sh (HMGB1) mice. Scale bar=75 μm. (B) Corresponding semiquantification of HMGB1 mRNA expression level in different groups and (C) percentile of astrocytes (n = 3 mice/group). (D) Western blotting (E) and quantification of HMGB1, VEGFA and FGF2, protein levels (from left to right, normalised to corresponding sham) in ipsilateral mice brain, n=4 mice/group for all groups. (F) mNSS, (G) tail suspension, (H) grid walking and (I) rotarod test of neurobehavioural outcomes in each group (n=3 mice/group in sham groups, n=12 mice/group in the IS groups). IS, ischaemic stroke mice; IS US, ischaemic stroke mice treated with US; US, mice treated with ultrasound. Data are mean ± SD. LIFUS, low-intensity focused ultrasound stimulation.

We investigated the CAMK2N1 localisation and expression by FISH and Western blot (figure 5). FISH results showed that CAMK2N1 expressed in astrocytes at 14 days after MCAO (figure 5A). CAMK2N1 expression was downregulated in the IS US group compared with the IS group at 14 days after MCAO, and successfully increased in the IS US sh and the IS US gf-sh groups compared with the IS US control (figure 5B). Quantification of the number of CAMK2N1$^+$/GFAP$^+$ astrocytes showed that 80% of CAMK2N1$^+$ cells were astrocytes and 20% of CAMK2N1$^+$ cells were other cells in the perifocal regions at 14 days after MCAO (figure 5C).

Western blot analysis showed that CAMK2N1 was downregulated in the IS US groups compared with the IS group, which was reversed in the IS US CAMK2N1 (CAMK2N1 overexpression in the whole brain) and the IS US gf-CAMK2N1 (CAMK2N1 overexpression in astrocytes) groups (figure 5D,E). Meanwhile, IS US groups exhibited higher expression of Phospho-Ca^{2+}/calmodulin-dependent protein kinase II (p-CAMK2),

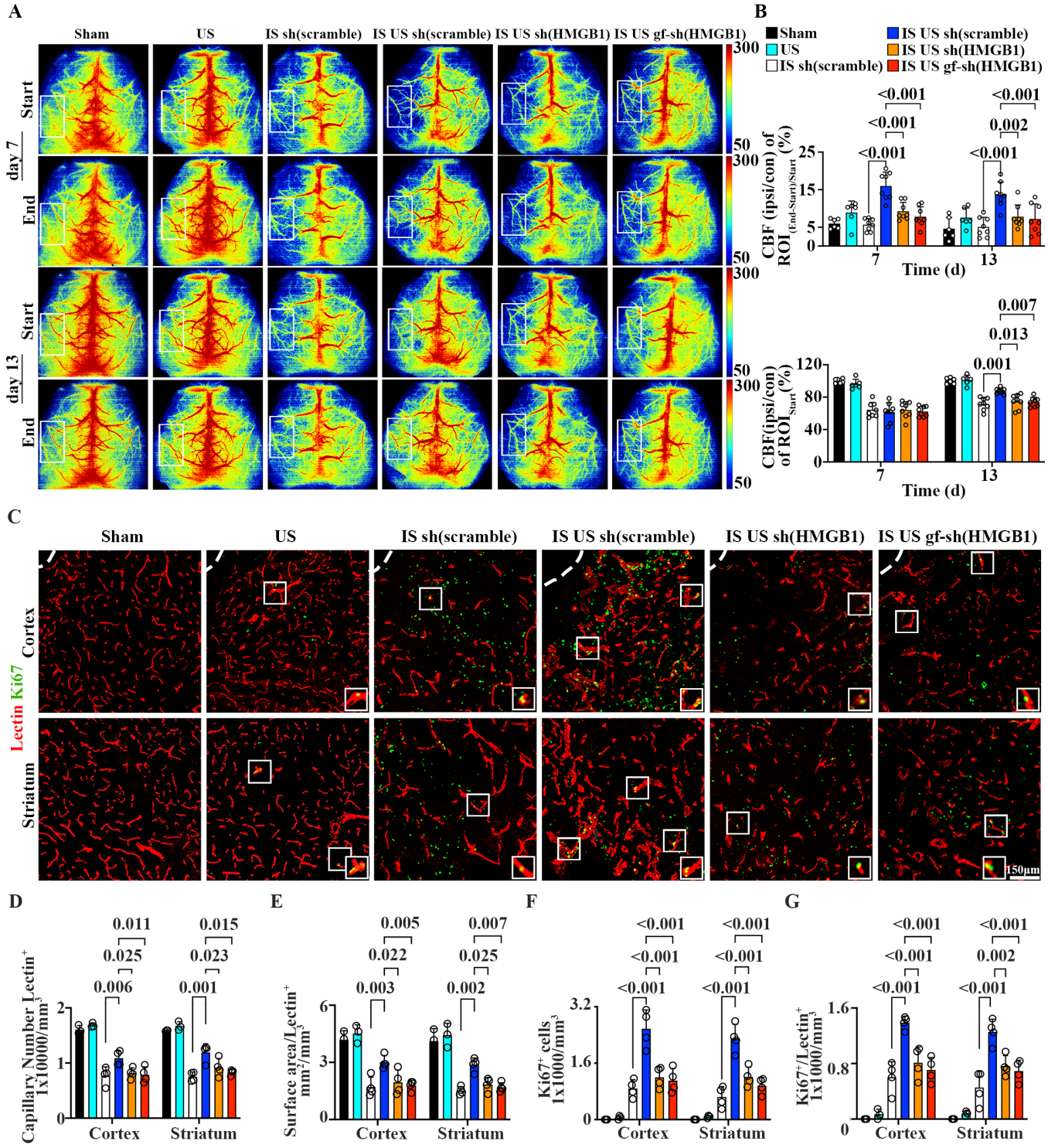

Figure 4 LIFUS upregulated astrocytic HMGB1 via increased CBF and lectin$^+$ microvessels in MCAO mice. (A) Representative images showed immediate CBF changes and endpoint CBF of ROI at 7 days and 13 days by laser speckle imaging in the sham, sham US, IS scramble, IS US scramble, IS US sh (HMGB1), IS US gf-sh (HMGB1) groups. (B) Quantification of CBF normalised to sham. Start row was the quantification of CBF at 7 days and 13 days, respectively. End row was the quantification of immediate CBF changes followed ultrasound at 7 days and 13 days respectively, (n=6 mice/group in the sham groups, n=10 mice/group in the IS groups). (C) Representative lectin (red) and Ki67 (green) immunostaining images, scale bar=150 μm. (D) Quantitative analysis of capillary number, (E) surface area showing angiogenesis in perifocal region. (F) Quantification of the Ki67$^+$ cells and (G) Ki67$^+$/lectin$^+$ signals to exhibit newly formed endothelial cells and microvessels, (n=3 mice/group in sham groups, n=4 mice/group in the IS groups). Sham groups indicated sham group and US group. IS groups indicated IS scramble group, IS US scramble group, IS US sh(HMGB1) group and IS US gf-sh (HMGB1) group. Data are mean ± SD. IS, ischaemic stroke mice; IS US, ischaemic stroke mice treated with US; US, mice treated with ultrasound; LIFUS, low-intensity focused ultrasound stimulation.

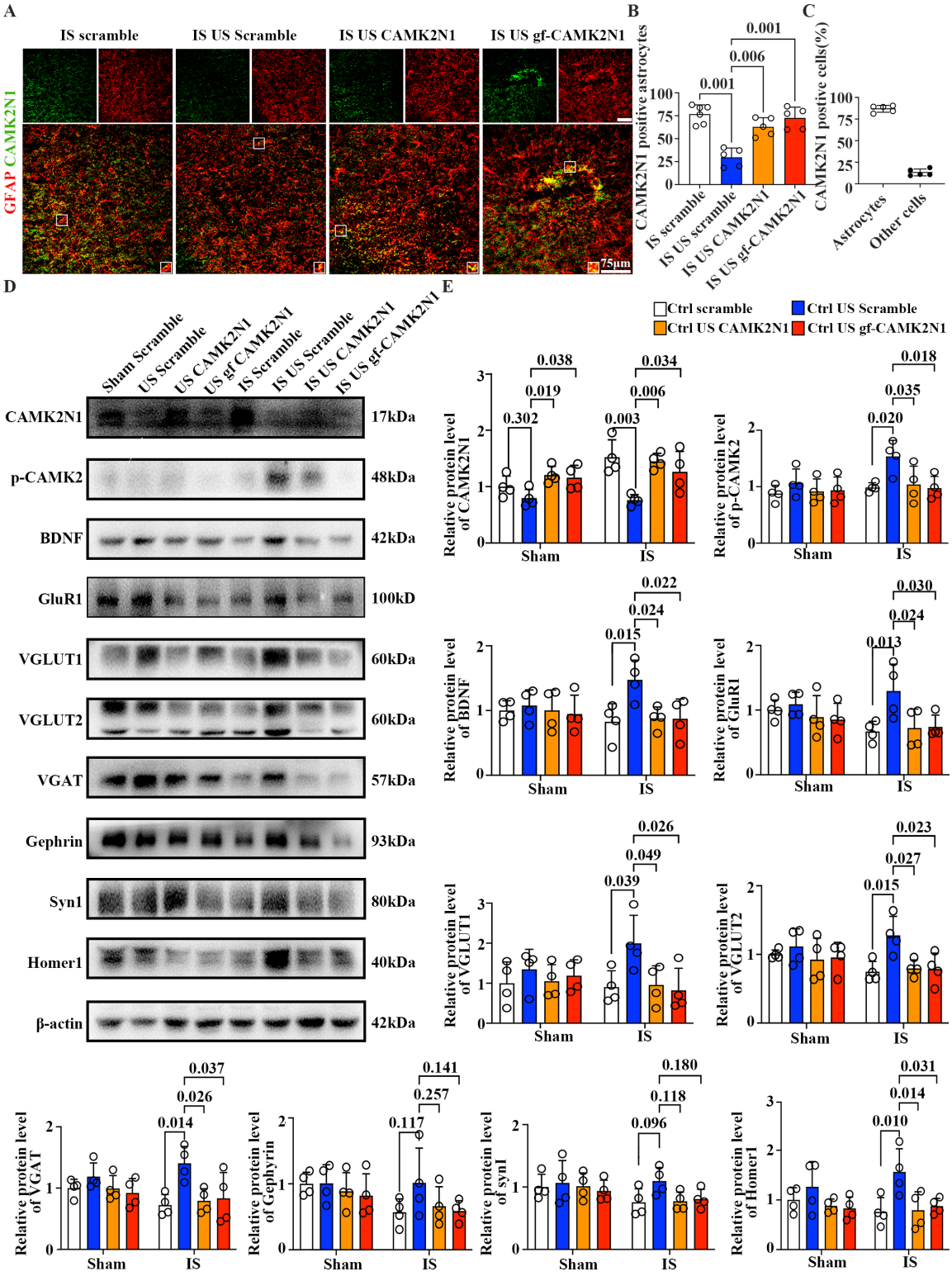

Figure 5 Astrocytic CAMK2N1 overexpression reversed the synapses increase after LIFUS in MCAO mice. (A) Representative images of CAMK2N1 (green) signals and GFAP+ astrocytes (red) in IS scramble, IS US scramble, IS US CAMK2N1, and IS US gf-CAMK2N1 mice. Scale bar = 75 μm. (B) Corresponding quantification of CAMK2N1 mRNA expression level in different groups and (C) percentile of astrocytes, (n= 3 mice/group). (D) Western blotting and (E) quantification of CAMK2N1, p-CAMK2, BDNF, GluR1, VGLUT1, VGLUT2, VGAT, Gephyrin, SynI, Homer1, respectively, from left to right and up to down, relative to β-actin and normalised to corresponding sham in ipsilateral hemisphere of mouse brain, (n=4 mice/group). Sham groups indicated sham scramble group, US group, US CAMK2N1 group and US gf-CAMK2N1 group. IS groups indicated IS scramble group, IS US scramble group, IS US sh (HMGB1) group and IS US gf-sh (HMGB1) group. Data are mean ± SD. IS, ischaemic stroke mice; IS US, ischaemic stroke mice treated with US; US, mice treated with ultrasound; LIFUS, low-intensity focused ultrasound stimulation.

which was also reversed after CAMK2N1 overexpression (figure 5E). In addition, LIFUS increased BDNF, excitatory synapse-related protein glutamate receptor 1 (GluR1), VGLUT1 and VGLUT2 expression. Inhibitory synapse protein (VGAT and Gephyrin), and total synapse protein (Synapsin I and Homer1) had similar expression pattern (figure 5E). At the same time, CAMK2N1 overexpression did not affect other protein expression or neurobehaviour in the sham mice (online supplemental figure 4G–L).

LIFUS-driven astrocytic CAMK2N1 downregulation promoted electrical signals and increased dendritic spine density after MCAO

To investigate morphological changes in neuron after increased synaptic protein levels, we performed Golgi-Cox staining to visualise neuronal dendritic spines in the peri-focal region (figure 6A). The number of total spines on secondary dendrites was shown and calculated (figure 6B). Results showed that the number of total spines was significantly increase in the IS US group compared with the IS group, which was reversed in the IS US CAMK2N1 and the IS US gf-CAMK2N1 groups compared with the IS US groups (figure 6C), suggesting that inhibition of downregulated CAMK2N1 in whole brain or astrocyte was beneficial for dendritic spines increase after ischaemic stroke.

Since GluR1 is a calcium-permeable neurotransmitter receptor and plays a key role in synaptic plasticity, we also applied fibre photometry records to detect Ca^{2+} changes after LIFUS. The results showed that frequency change of the calcium signals slightly increased in the US group (figure 6D), while it was significantly higher in the IS US groups than that in the IS, IS US CAMK2N1 and IS US gf-CAMK2N1 groups during 3-min LIFUS (figure 6E). Heatmap displayed variance of three mice in one group, suggesting that there was a relatively strong increase of frequency after LIFUS, and this enhancement could be reversed by CAMK2N1 overexpression in whole brain cells and astrocytes (figure 6F,G). Furthermore, we also evaluated nerve-to-muscle signal transmission of motor neurons by electromyography (EMG) amplitude. Results showed that the amplitude increased during LIFUS both in the US and the IS US groups at day 7 and day 13 after MCAO, which was consistent with Ca^{2+} level changes in the brain. LIFUS-induced enhancements were inhibited in US CAMK2N1 and US gf-CAMK2N1 groups (figure 6H–K). Calcium signals frequency and EMG amplitude of original waves were stable before LIFUS in the different groups (online supplemental figure 5). These results suggested that LIFUS induced calcium changes and increased neuronal activities. Neurobehavioural outcomes including the mNSS, tail suspension test, grid walking and rotarod test were better in the IS US group than that in the IS US CAMK2N1 and IS US gf-CAMK2N1 groups of mice (figure 6L–O). The recovery was reversed by CAMK2N1 overexpression in the whole brain and astrocytes.

DISCUSSION

In this study, we demonstrated that LIFUS enhanced HMGB1 expression in a subcluster of astrocytes of ischaemic mouse brain, which promoted microvasculature repair and remodelling. At the same time, downregulated CAMK2N1 increased neural dendritic spines and synapse generation, which eventually leads to neurological functional recovery. We highlighted a molecularly targeted mechanism for the LIFUS therapy at the single-cell level and implies a therapeutic rationale for neurogenesis, angiogenesis and synaptogenesis for the preclinical trials, and provided a theoretical basis for LIFUS to be applied to other diseases.

Previous studies showed that LIFUS with 400 mW/cm^2 preconditioning mitigated focal cerebral ischaemia in rats.[26] LIFUS pretreatment could also significantly decrease the neuronal cell apoptosis, downregulation of apoptosis-related signalling molecules and upregulation of BDNF in the ischaemic brain tissue with I_{spta}=528 mW/cm^2.[27] It is noted that I_{sppa} = 39 mW/cm^2 for mice[22] or I_{sppa} = 2.6 W/cm^2[28] for rats in the post ischaemic stage were proved protective when LIFUS with 12-hour or 24-hour interval. LIFUS with 193 mW/cm^2 used to the whole brain 3 times in the first week after MCAO upregulated neurotrophies including VEGF and eNOS.[20] Our study supported that 3 min with 101 mW/cm^2 every other day was optimal ultrasound parameter for neurorehabilitation in the late acute stage (after 7 days) of MCAO, which provided a safe and effective treatment for ischaemic stroke.

Based on proteomic protein expression and enrichment pathways, we set the indicators as angiogenesis and synaptogenesis, the key factor for stroke recovery, to observe the effects of ultrasound stimulation. Therefore, we first considered the components of neurovascular units, including astrocyte end-foot, endothelium, pericytes, neurons and microglia.[29–31] Microglia-enriched pathways mainly promote inflammation and immune-related functions, neurons and endothelial cell are the target cell for angiogenesis and synaptogenesis, astrocytes are cardinal mediator between neurons and endothelial cells, and played a vital role in the neurovascular unit remodelling after ischaemic stroke.[32 33] Astrocyte-mediated neurovascular coupling signals could stimulate neurons, leading to a calcium efflux and release of vasoactive substances onto vessels.[34–37] Increasing evidence showed that astrocytes are major cell type affected by ultrasound.[18 38] At the same time, we observed significant changes of HMGB1 and CAMK2N1 in ischaemic mice after ultrasound only in astrocytes, but not in other cells, which intrigue us to conduct cellular level experiments and related validation in astrocytes.

We also found that angiogenesis and neurogenesis (synaptogenesis) are the most significantly enriched pathways in proteomic analysis by ultrasound stimulation after stroke, then HMGB1 and CAMK2N1 were identified as the most significantly differential genes in both pathways. Furthermore, we performed scRNA sequencing to further

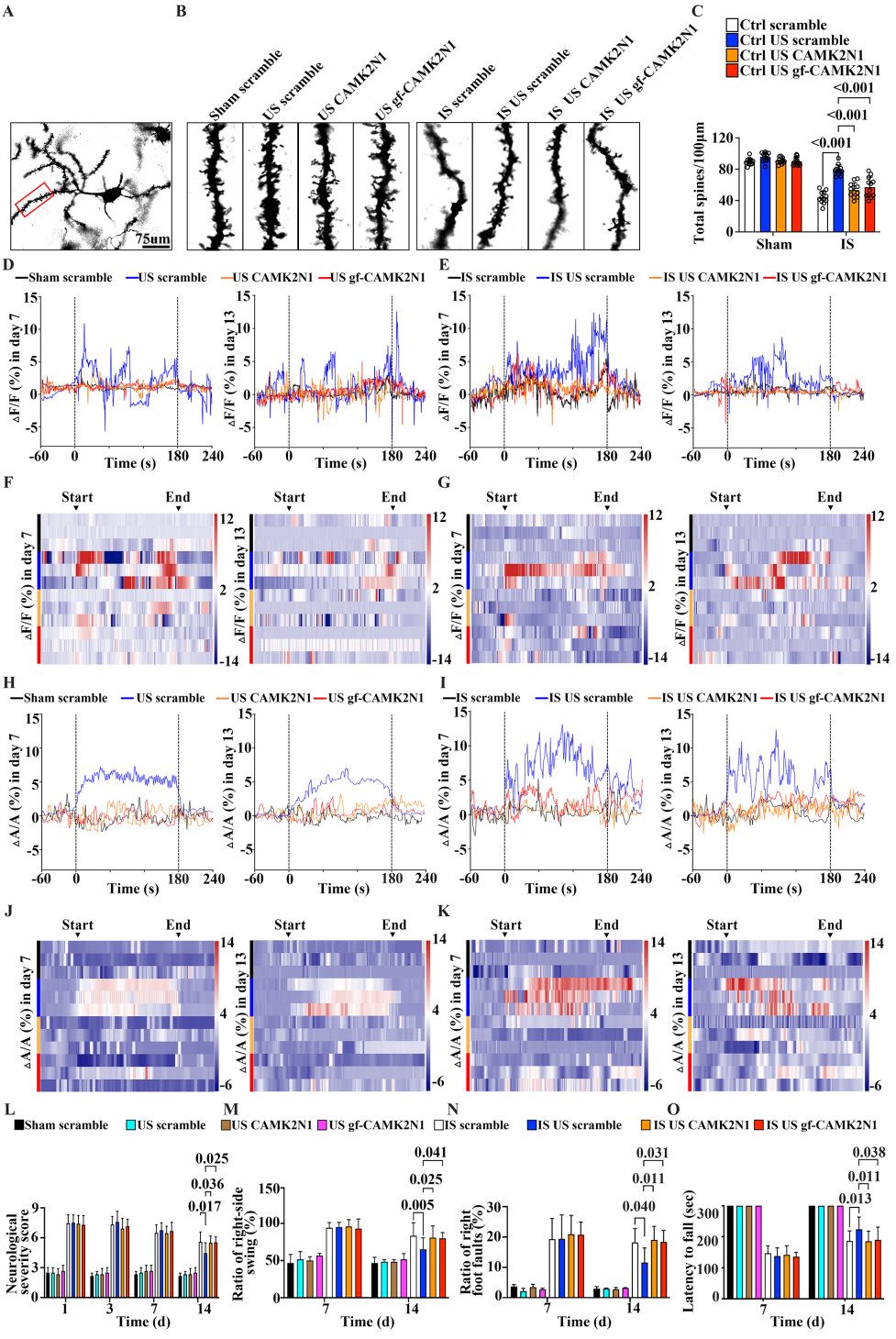

Figure 6 Astrocytic CAMK2N1 downregulated by LIFUS promoted electrical signals and increased dendritic spine density after LIFUS in MCAO mice. (A) Presentative Golgi staining images and quantitative analysis. Low magnification of Golgi staining images of neurons in the perifocal region of ipsilateral hemisphere. Scale bar=75 μm. (B) Representative images of dendritic spines and (C) a bar graph showed the number of total spines in the sham, US, US CAMK2N1, US gf-CAMK2N1, IS, IS US, IS US CAMK2N1, IS US gf-CAMK2N1 mice at 14 days after MCAO, (n=4 mice/group). (D) Average $Ca2^{+}$ transients (detla F/F) and (E) variance of GCaMP6s signals were displayed at day 7 and day 13 after MCAO. (F) and (G) Heatmap displayed variance of the calcium activity of neurons during a 5-min records after ultrasound stimulation and CAMK2N1 overexpression respectively (n=3 mice/group). (H, I) Electromyography (EMG) records showed average EMG amplitude (detla A/A) and (J, K) variance heatmap during a 5-min records, (n=3 mice/group). (L) mNSS, (M) tail suspension, (N) grid walking (O) and rotarod test showed that neurobehavioural outcomes in different groups, (n=3 mice/group in the sham groups, n=12 mice/group in the IS groups). Ctrl (black line), Ctrl US (blue line), Ctrl US CAMK2N1 (yellow line), and Ctrl US gf-CAMK2N1 (red line) mice. Data are mean ± SD. IS, ischaemic stroke mice; IS US, ischaemic stroke mice treated with US; US, mice treated with ultrasound; LIFUS, low-intensity focused ultrasound stimulation.

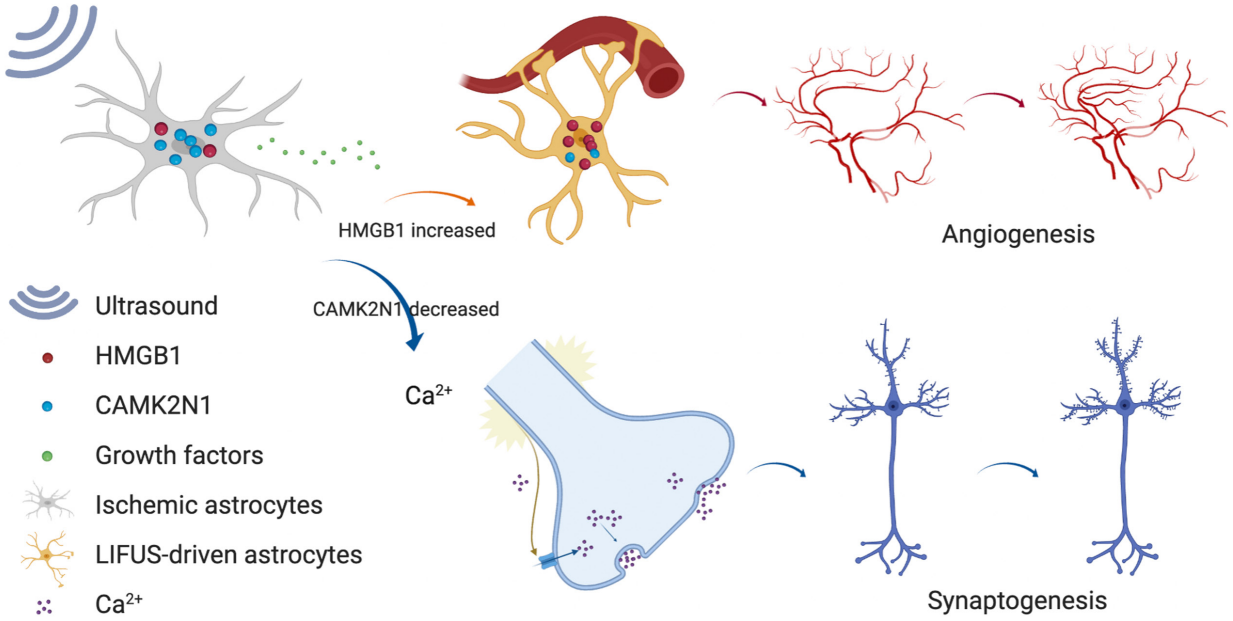

Figure 7 Low-intensity focused ultrasound stimulation promotes stroke recovery via astrocytic HMGB1 and CAMK2N1 in mice. LIFUS, low-intensity focused ultrasound stimulation.

identify ultrasound-induced post-stroke changes at the cellular level, as well as pathways affected by ultrasound stimulation. Interestingly, we demonstrated that HMGB1 and CAMK2N1 are also the significantly changed genes in astrocytes. Previous studies showed that ultrasound stimulation mediated by astrocytes to promote angiogenesis and synaptogenesis, and HMGB1[39 40] and CAMK2N1[41 42] involved in this process. Therefore, we identified these two genes as targets for further experiments. Overall, HMGB1 and CAMK2N1 are the overlapping targets of proteomics and scRNA sequencing in ischaemic stroke mice, which promoted angiogenesis and synaptogenesis after ultrasound stimulation. Other studies showed that HMGB1 could release from astrocytes for neurovascular remodelling and angiogenesis through TLR4 and RAGE signalling pathways after ischaemic injury.[43 44] CAMK2 (calcium/calmodulin-dependent protein kinase 2) was critical for transducing Ca^{2+} signals and contributing to cellular calcium homeostasis after injury. In our study, LIFUS promoted angiogenesis-related genes' expression including PECAM1 and VEGFR1/Flt1 in both iTRAQ proteomics and scRNA-seq. Furthermore, LIFUS also promoted synaptogenesis-related genes like Atp5f1, Gabarap, Nyap1, Ryr3 and Trpv2, which could increase Ca^{2+} influx compared with IS groups. Increased brain calcium could activate or lead to a high concentration of CAMK2 translocases from the dendritic shaft to postsynaptic densities of dendritic spines, which played a critical role in calcium signalling regulation in learning and synaptic plasticity, and cell proliferation. CAMK2N1 translocated from the nuclei to the cytoplasm could directly interact with CAMK2[45] to inhibit its phosphorylation, and CAMK2N1-CAMK2 signalling restricts synaptic progression.

Clinical transformation and application are very important for the LIFUS. In fact, research on LIFUS for CNS disease therapy is still in the laboratory and preclinical stage (fusfoundation.org), especially in ischaemic stroke. Animal studies help to understand the efficacy, safety and the underlying mechanism. In addition, this research proved ultrasound stimulation could promote neurological function and physical rehabilitation, which provides an opportunity to treat patients who remain disabled after thrombolysis. We also have a series of further studies to explore the mechanism of ultrasound stimulation, which will further provide significant translational value for clinical trials eventually. Our results provided preliminary in vivo data for the potential clinical application of small and convenient ultrasound instrument to the human body. The efficacy of ultrasound treatment in the subacute stage of stroke in animals could be expanded to the clinical use. In future, the movement rehabilitation in patients who had a stroke can not only from limb rehabilitation to brain recovery, but also can from central angiogenesis and synaptogenesis induced by ultrasound to the limb rehabilitation. The mechanism by which ultrasound acts on astrocytes to promote angiogenesis and synaptogenesis can also be used as an experimental technique basis for determining the specific brain region that ultrasound stimulate in subsequent studies. In addition, our study provides an important reference for ultrasound treatment of neurodegenerative diseases such as Alzheimer's Disease (AD), Parkinson's disease (PD) and other brain diseases such as glioma.

CONCLUSIONS

Our findings suggest that LIFUS therapy promoted angiogenesis and synaptogenesis via astrocytic HMGB1 and

CAMK2N1 (Figure 7). The results highlight a molecularly targeted mechanism for LIFUS therapy at the single-cell level, which provided a deeper understanding about the key molecular and cellular events of LIFUS-induced recovery after ischaemic stroke, and theoretical basis for extending LIFUS to other disease models and clinical settings.

Author affiliations
[1]Shanghai Jiao Tong Affiliated Sixth People's Hospital, School of Biomedical Engineering, Shanghai Jiao Tong University, Shanghai, Shanghai, China
[2]Department of Neurosurgery, Huashan Hospital, Shanghai Medical Collage, Fudan University, Shanghai, China
[3]Department of Neurosurgery, Shanghai Sixth People's Hospital Affiliated to Shanghai Jiao Tong University, Shanghai, China
[4]Paul C. Lauterbur Research Center for Biomedical Imaging, Shenzhen Institutes of Advanced Technology, Chinese Academy of Sciences, Beijing, China
[5]Neuroscience and Neuroengineering Center, Shanghai Jiao Tong University School of Biomedical Engineering, Shanghai, China
[6]Shanghai Jiao Tong University Medical School Affiliated Ruijin Hospital, Shanghai, China

Contributors ZZ is responsible for the overall content. G-YY, ZZ, and JW conceived the project, designed the experiments, and edited the paper finally. LQ designed and performed the experiments, analysed the data, and drafted the manuscript and figures. CW participated in scRNA-seq, FISH, and data analysis. LD and J-JP contributed to behaviour tests and immunostaining. QS and SW helped with sample collection. XS, JS and WQ contributed to ultrasound parameter design, electromyogram and fiber photometry records. LC contributed to the western blot. YT, and YW helped to design the experiment and interpret the data.

Funding This study was supported by grants from the Scientific Research and Innovation Program of Shanghai Education Commission 2019-01-07-00-02-E00064 (G-YY), the National Natural Science Foundation of China 82271320 (ZZ), 82172529 (WJ), 81974179 (ZZ), 82071284 (YT), Scientific and Technological Innovation Act Program of Shanghai Science and Technology Commission, 20JC1411900 (G-YY), National Key R&D Program of China 2022YFA1603604 (ZZ), 2019YFA0112000 (YT), 2018YFA0701400 (WQ) and 2021ZD0200401 (WQ), Shenzhen Foundation Grant JCYJ20200109114237902 (WQ), SGDX2020110309400200 (WQ).

Competing interests None declared.

Patient consent for publication Not applicable.

Ethics approval Not applicable.

Provenance and peer review Not commissioned; externally peer reviewed.

Data availability statement Data are available in a public, open access repository. All data relevant to the study are included in the article or uploaded as supplementary information. Data are available upon reasonable request.

ORCID iDs
Yongting Wang http://orcid.org/0000-0002-5841-6557
Guo-Yuan Yang http://orcid.org/0000-0003-3105-9307
Jixian Wang http://orcid.org/0000-0002-3660-3175

REFERENCES

1 Campbell BCV, Khatri P. Stroke. *Lancet* 2020;396:129–42.
2 Blackmore J, Shrivastava S, Sallet J, *et al*. Ultrasound neuromodulation: a review of results, mechanisms and safety. *Ultrasound Med Biol* 2019;45:1509–36.
3 Darmani G, Bergmann TO, Butts Pauly K, *et al*. Non-invasive transcranial ultrasound stimulation for neuromodulation. *Clin Neurophysiol* 2022;135:51–73.
4 Patabendige A, Singh A, Jenkins S, *et al*. Astrocyte activation in neurovascular damage and repair following ischaemic stroke. *Int J Mol Sci* 2021;22:4280.
5 Bartus K, Galino J, James ND, *et al*. Neuregulin-1 controls an endogenous repair mechanism after spinal cord injury. *Brain* 2016;139:1394–416.
6 Bystritsky A, Korb AS, Douglas PK, *et al*. A review of low-intensity focused ultrasound pulsation. *Brain Stimul* 2011;4:125–36.
7 Yu K, Niu XD, Krook-Magnuson E, *et al*. Intrinsic functional neuron-type selectivity of transcranial focused ultrasound neuromodulation. *Nat Commun* 2021;12:2519.
8 Hummel FC, Cohen LG. Non-invasive brain stimulation: a new strategy to improve neurorehabilitation after stroke *Lancet Neurol* 2006;5:708–12.
9 Yuan Y, Wang Z, Liu M, *et al*. Cortical hemodynamic responses induced by low-intensity transcranial ultrasound stimulation of mouse cortex. *Neuroimage* 2020;211.
10 Marsac L, Chauvet D, Larrat B, *et al*. MR-guided adaptive focusing of therapeutic ultrasound beams in the human head. *Med Phys* 2012;39:1141–9.
11 Zibly Z, Graves CA, Harnof S, *et al*. Sonoablation and application of MRI guided focused ultrasound in a preclinical model. *J Clin Neurosci* 2014;21:1808–14.
12 Wang Z, Yan J, Wang X, *et al*. Transcranial ultrasound stimulation directly influences the cortical excitability of the motor cortex in parkinsonian mice. *Mov Disord* 2020;35:693–8.
13 Landhuis E. Ultrasound for the brain. *Nature* 2017;551:257–9.
14 de Lucas B, Pérez LM, Bernal A, *et al*. Ultrasound therapy: experiences and perspectives for regenerative medicine. *Genes (Basel)* 2020;11:1086.
15 Shindo T, Ito K, Ogata T, *et al*. Low-intensity pulsed ultrasound enhances angiogenesis and ameliorates left ventricular dysfunction in a mouse model of acute myocardial infarction. *Arterioscler Thromb Vasc Biol* 2016;36:1220–9.
16 Hanawa K, Ito K, Aizawa K, *et al*. Low-intensity pulsed ultrasound induces angiogenesis and ameliorates left ventricular dysfunction in a porcine model of chronic myocardial ischemia. *PLoS One* 2014;9:e104863.
17 Barzelai S, Sharabani-Yosef O, Holbova R, *et al*. Low-intensity ultrasound induces angiogenesis in rat hind-limb ischemia. *Ultrasound Med Biol* 2006;32:139–45.
18 Liu SH, Lai YL, Chen BL, *et al*. Ultrasound enhances the expression of brain-derived neurotrophic factor in astrocyte through activation of Trkb-AKT and calcium-CaMK signaling pathways. *Cereb Cortex* 2017;27:3152–60.
19 Chen L, Zheng Q, Chen X, *et al*. Low-frequency ultrasound enhances vascular endothelial growth factor expression, thereby promoting the wound healing in diabetic rats. *Exp Ther Med* 2019;18:4040–8.
20 Ichijo S, Shindo T, Eguchi K, *et al*. Low-intensity pulsed ultrasound therapy promotes recovery from stroke by enhancing angio-neurogenesis in mice in vivo. *Sci Rep* 2021;11:4958.
21 Karmacharya MB, Kim KH, Kim SY, *et al*. Low intensity ultrasound inhibits brain oedema formation in rats: potential action on AQP4 membrane localization. *Neuropathol Appl Neurobiol* 2015;41:e80–94.
22 Deng L-D, Qi L, Suo Q, *et al*. Transcranial focused ultrasound stimulation reduces vasogenic edema after middle cerebral artery occlusion in mice. *Neural Regen Res* 2022;17:2058–63.
23 Radchenko EV, Tarakanova AS, Karlov DS, *et al*. Ligands of the AMPA-subtype glutamate receptors: mechanisms of action and novel chemotypes. *Biomed Khim* 2021;67:187–200.
24 Sun P, Zhang K, Hassan SH, *et al*. Endothelium-targeted deletion of microRNA-15A/16-1 promotes poststroke angiogenesis and improves long-term neurological recovery. *Circ Res* 2020;126:1040–57.
25 Wang C, Yang X, Jiang Y, *et al*. Targeted delivery of fat extract by platelet membrane-cloaked nanocarriers for the treatment of ischemic stroke. *J Nanobiotechnology* 2022;20:249.
26 Li H, Sun J, Zhang D, *et al*. Low-intensity (400 mW/cm^2, 500 kHz) pulsed transcranial ultrasound preconditioning may mitigate focal cerebral ischemia in rats. *Brain Stimul* 2017;10:695–702.
27 Chen CM, Wu CT, Yang TH, *et al*. Preventive effect of low intensity pulsed ultrasound against experimental cerebral ischemia/

reperfusion injury via apoptosis reduction and brain-derived neurotrophic factor induction. *Sci Rep* 2018;8.
28 Liu L, Du J, Zheng T, *et al*. Protective effect of low-intensity transcranial ultrasound stimulation after differing delay following an acute ischemic stroke. *Brain Res Bull* 2019;146:22–7.
29 Schaeffer S, Iadecola C. Revisiting the neurovascular unit. *Nat Neurosci* 2021;24:1198–209.
30 Otsu Y, Couchman K, Lyons DG, *et al*. Calcium dynamics in astrocyte processes during neurovascular coupling. *Nat Neurosci* 2015;18:210–8.
31 Kaplan L, Chow BW, Gu C. Neuronal regulation of the blood-brain barrier and neurovascular coupling. *Nat Rev Neurosci* 2020;21:416–32.
32 Poskanzer KE, Molofsky AV. Dynamism of an astrocyte in vivo: perspectives on identity and function. *Annu Rev Physiol* 2018;80:143–57.
33 Mishra A, Hamid A, Newman EA. Oxygen modulation of neurovascular coupling in the retina. *Proc Natl Acad Sci U S A* 2011;108:17827–31.
34 Mishra A, Reynolds JP, Chen Y, *et al*. Astrocytes mediate neurovascular signaling to capillary pericytes but not to arterioles. *Nat Neurosci* 2016;19:1619–27.
35 Attwell D, Buchan AM, Charpak S, *et al*. Glial and neuronal control of brain blood flow. *Nature* 2010;468:232–43.
36 Mulligan SJ, MacVicar BA. Calcium transients in astrocyte endfeet cause cerebrovascular constrictions. *Nature* 2004;431:195–9.
37 Takano T, Tian G-F, Peng W, *et al*. Astrocyte-mediated control of cerebral blood flow. *Nat Neurosci* 2006;9:260–7.
38 Deng Z, Wang J, Xiao Y, *et al*. Ultrasound-mediated augmented exosome release from astrocytes alleviates amyloid-beta-induced neurotoxicity. *Theranostics* 2021;11:4351–62.
39 He H, Wang X, Chen J, *et al*. High-mobility group box 1 (HMGB1) promotes angiogenesis and tumor migration by regulating hypoxia-inducible factor 1 (HIF-1Alpha) expression via the phosphatidylinositol 3-kinase (PI3K)/AKT signaling pathway in breast cancer cells. *Med Sci Monit* 2019;25:2352–60.
40 Biscetti F, Straface G, De Cristofaro R, *et al*. High-mobility group Box-1 protein promotes angiogenesis after peripheral ischemia in diabetic mice through a VEGF-dependent mechanism. *Diabetes* 2010;59:1496–505.
41 Peng J-M, Tseng R-H, Shih T-C, *et al*. CAMK2N1 suppresses hepatoma growth through inhibiting E2F1-mediated cell-cycle signaling. *Cancer Lett* 2021;497:66–76.
42 Bhattacharyya M, Karandur D, Kuriyan J. Structural insights into the regulation of Ca(2+)/calmodulin-dependent protein kinase II (CaMKII). *Cold Spring Harb Perspect Biol* 2020;12:a035147.
43 Yang S, Xu L, Yang T, *et al*. High-mobility group box-1 and its role in angiogenesis. *J Leukoc Biol* 2014;95:563–74.
44 Zhu L, Ren L, Chen Y, *et al*. Redox status of high-mobility group box 1 performs a dual role in angiogenesis of colorectal carcinoma. *J Cell Mol Med* 2015;19:2128–35.
45 He Q, Li Z. The dysregulated expression and functional effect of CaMK2 in cancer. *Cancer Cell Int* 2021;21:326.